Colloid Polym Sci 279:221–231 (2001)

ORIGINAL CONTRIBUTION

J. Simola-Gustafsson
B. Hortling
J. Peltonen

Scanning probe microscopy and enhanced data analysis on lignin and elemental-chlorine-free or oxygen-delignified pine kraft pulp

Received: 17 March 2000
Accepted: 1 September 2000

J. Simola-Gustafsson (✉) · J. Peltonen
Department of Physical Chemistry
Åbo Akademi University
Porthansgatan 3-5, 20500 Turku, Finland
e-mail: jsimola@abo.fi
Tel.: +358-2-2154252
Fax: +358-2-2154706

B. Hortling
The Finnish Pulp and Paper Research Institute (KCL), POB 70
02151 Espoo, Finland

Abstract Fibres from conventional pine kraft pulp (KP), oxygen-delignified KP (KPO) and elemental-chlorine-free (ECF) bleached KP were characterized by scanning probe microscopy (SPM). The surface morphology of lignin isolated from the respective pine KP was studied. The data analysis of the phase-shift data measured by using different tapping mode imaging parameters enabled the study of both the surface amphiphility and stiffness as a function of delignification. The average phase-shift values were observed to correlate to the respective kappa values, when imaging with small tapping amplitude (30 nm), referred to the capability of SPM to follow local amphipilic (adhesion) differences on a wood fibre surface. The roughness (standard deviation) of the average phase-shift values was taken as a measure of the sample homogeneity. The mean morphological roughness was observed to increase with decreasing bulk lignin concentration. The surface of lignin appeared mainly granular but occasionally some linear structures were observed. The surface roughness of different fractions of flow-through residual lignin samples correlated quite well to the molar mass of the respective fraction. Each grain contained hundreds of lignin molecules. Most of the lignin samples were homogeneous as regards friction and phase-contrast images. The surface of the nondelignified pine KP was typically granular. ECF delignification was more effective than oxygen delignification in removing this granular phase. The decrease in the relative amount of the granular phase correlated to a decreasing kappa value of the pulp. The granular phase is thus suggested to correspond to lignin, but it cannot be ruled out that small amounts of hemicellulose, extractives or a mixture of these components are embedded in this phase. The surface concentration of the granular phase of the KPO samples was, according to the phase-contrast images, clearly higher than the bulk lignin concentration, as indicated by the corresponding kappa values.

Key words Wood fibres · Lignin · Scanning probe microscopy · Phase-contrast imaging

Introduction

Wood consists mainly of polymeric constituents, i.e. cellulose, hemicelluloses and lignin. Native cellulose is a linear (about 5 μm) homopolysaccharide of β-(1-4)-linked D-glucopyranose moieties aligned in bundles, so-called microfibrils of 100–500 cellulose chains. Hemicelluloses such as xylan, glucomannan and galactan are slightly branched heteropolysaccharides. Lignin consists of phenylpropane units which are linked

together in random fashion. Lignin binds cellulose fibrils in the cell wall and links the cells in wood together, giving strength to the matrix [1, 2].

Cellulose makes up about half of the material in both softwood and hardwood. In woods of northern Europe, the lignin content is about 30 wt% for softwood and about 20 wt% for hardwood. The hemicellulose content is about 30 wt% for both species. The amount of the extractives varies in the springwood and summerwood and is characteristic for different trees, for example, for pine it is about 2.5–4.8% [2]. Chemically, the components of wood can be distinguished; however, the exact chemical structure of lignin is still unknown. The research on the topography has mostly focused on cellulose, for which the knowledge has improved through the advancement of experimental techniques [3–7].

Most problems in analysis of lignin relate to the modification of its structure during extraction (cooking and delignification). Changes in morphology during the chemical transformation of lignin into low-molar-mass degradation products, kraft lignins and humic substances are a result of changes in chemical structure and properties. It has been suggested that the actual morphology and chemical behaviour of lignins and related polymers under pulping and environmental conditions are strongly influenced by the surrounding polar matrices, which may be either organic or inorganic [8]. Several reasons make the study of wood samples complicated. The structure and relative proportions of different wood components differ in the various parts of a tree. The varying number and size of the pits in different trees contribute to the structure. The softwood lignin and hemicelluloses differ from lignin and hemicelluloses of hardwood. The surface of pulp fibres changes considerably during the delignification process owing to chemical reactions, dissolution of lignin and hemicellulose and readsorption of different compounds from the process liquors [2, 9, 10]. Thus, the topographical investigations of the fibre surface and isolated lignin yield new information about the structural changes of lignin in extraction processes and helps to understand how the surface of the fibres is modified as a result of different cooking and delignification methods.

Scanning probe microscopy (SPM) [11] creates a surface image by scanning a flexible cantilever with a mounted tip over the sample. The torsional deflection of the tip is proportional to the lateral friction forces acting on the cantilever during scanning. Recording a 2D map of this torsion is termed friction force microscopy (FFM) [12–14]. Local differences in the frictional force refer to inhomogeneities in the surface material or edge effects arising from abrupt changes in the height profile of the surface.

The phase-imaging technique is an extension of the tapping-mode SPM, where a cantilever is excited into resonance oscillation with a piezoelectric driver and the oscillation amplitude is used as a feedback signal to track the surface topography. The phase angle of the oscillating cantilever with respect to that of the piezoelectric driver changes when the probe encounters surface regions of different adhesion, stiffness or viscoelastic composition. Besides the surface properties of the sample studied the amount and direction (sign) of the phase shift is dependent on the free amplitude of tapping, A_0, the measuring frequency, f, and the damping ratio, $r_{sp} = A_{sp}/A_0$ (A_{sp} equals the imaging set-point amplitude). With small A_0 and large r_{sp} values the attractive forces (e.g. adhesion and capillary forces) leading to negative phase shift dominate the tip–sample interaction. With these measuring parameters the tip-contamination layer interaction is significant compared to the relatively weak tip–sample surface interaction. Because the water content of the surface dominates the contamination layer, the more hydrophilic the surface region the more negative the observed phase shift (i.e. darker contrast in SPM image). With large A_0 and moderate to small r_{sp} values the tip–sample interaction turns to the repulsive regime. The tip–sample surface interaction dominates and the relative contribution arising from the contamination layer decreases. Thus, the phase-image contrast becomes related to the variation of the local elastic properties (i.e. stiffness) on the sample surface. The locally stiffer regions give a more positive phase shift (i.e. a lighter phase image) than the softer surface regions. In addition, inelastic tip–sample interaction with further increased forces leads to a longer tip–sample contact time and increasing contact area, which both increase [15] the phase shift.

Recently, phase imaging has been widely studied and applied [15–23], mostly for binary systems with predictable properties. Pulp fibre research with SPM has mainly focused on model celluloses on the nanometre scale and studies on the properties of the isolated polymers [5, 6, 8, 24]. In addition, sections of wood fibres have been imaged [25, 26]. Only little SPM work has been directed towards the other components of wood fibres [8, 27–29] or morphological changes on wood species of northern Europe during delignification. The study and development of phase-contrast imaging and the respective data analysis of wood fibres may enable us to follow the surface properties of fibres during different delignification processes.

For the pulp and paper industry it is essential to be able to relate the topographical and chemical structure of wood, i.e. to measure the interactions between the components of individual fibres. Determining and localizing the surface components of wood fibres would help to achieve this aim. The depolymerization of lignin is the main process in pulping technology and, therefore, the structure and chemical reactivity of lignin is of interest for both science and technology. In this study we

report an early mesoscopic scale characterization of Finnish pine fibres of conventional kraft pulp (KP) samples as a function of oxygen and elemental-chlorine-free (ECF) delignification and we compare these samples with pure lignin samples from the same pulp. The influence of the tapping amplitude on the phase shift data was studied and applied for the analysis of the adhesion (amphipilicity) and stiffness (hardness) properties of the samples studied.

Experimental

Preparation and properties of the pulps [30, 31]

The pine (*Picea abies*) KP was cooked at a liquor-to-wood ratio of 3.5, the effective alkali was 4.5 mmol/kg and the sulphidity was 35%. The temperature was raised from 20 to 80 °C at 2 °C/min, from 80 to 170 °C at 1 °C/min and kept at 170 °C for 120 min. The charge of the chips was 120 kg and a 600-l digester with forced-liquid circulation was used.

In flow-through KP (FTKP) the cooking liquor flowed through the pine chips (continuous exchange of the cooking liquor) with a flow rate of 70 ml/min. FTKP was prepared using an effective alkali of 0.50 mol/l and a sulphidity of 30%. The temperature was increased from 20 to 80 °C at 2 °C/min, kept at 80 °C for 30 min and increased form 80 to 170 °C at 1 °C/min. After that the temperature was kept at 170 °C for 2 h. In total, 21.8 l of the cooking liquor was used. The charge of the chips was 350 g and a 3-l digester was used.

The oxygen-delignified pulp (KPO) was prepared from KP with a consistency of 12.5%, a temperature of 95 °C, a NaOH concentration of 2.5% and at an oxygen pressure of 8 bar. The kappa number of the pulp was 15.4, the brightness 30.3% and the viscosity 950 ml/g. The kappa-number test is a standardized indirect method for determining the lignin content of pulps (ISO 302 standard). The brightness was determined according to the ISO 2470 standard and the viscosity according to the ISO 5351/1 standard.

The fully bleached pulp (BKP) was prepared from KPO using the bleaching sequence D0(EO)D1E2D2 (ECF delignification). In the D0 stage the consistency was 3%, the temperature 55 °C, the reaction time 60 min and the ClO_2 consumption 3.08% active chlorine(aCl). The EO stage was performed at a 12% consistency, 60 °C, an oxygen pressure of 2 bar and a NaOH concentration of 1.54%. In the D1 stage the consistency was 10%, the temperature 60 °C, the treatment time 180 min and the ClO_2 consumption 0.55% aCl. In the E2 stage the consistency was 10%, the temperature 60 °C, the time 60 min and the NaOH concentration 0.8%. The D2 stage was performed at a 10% consistency, 70 °C for 180 min and the ClO_2 consumption was 0.58% aCl. The brightness of the pulp was 89.3%, the viscosity 840 ml/g and the yield 95.8%.

Isolation and fractionation of residual lignins

The residual lignin (RL) isolated either from KP (KPRL) or FTKP (FTRL) was isolated by enzymatic hydrolysis using a mixture of a commercial cellulase and hemicellulases together with β-glucosidase as described earlier [32]. The lignin produced looked like dark-brown sand or powder particles. These were immobilized on the SPM sample stub by double-sided adhesive tape. Owing to the enzymatic isolation method the residual lignin contained 5 ± 1% protein contaminants and 6 ± 1% carbohydrates. The almost equal content of these components in the samples was assumed to have a similar, if any, effect on the SPM measurements. The residual lignin sample (100 mg) was reduced by $NaBH_4$ in order to stabilize the carbohydrate residues. The preparative gel permeation chromatography was then carried out using a HiLoad 20/60 Superdex 200 column (26 × 600 mm, Pharmacia Biotech) with 0.1 M NaOH as the eluant and a flow rate of 1 ml/min. A UV detector monitoring at 280 nm was used and 20-ml fractions were collected, from which the residual lignin samples were precipitated at pH 2.5, washed and freeze-dried. The content of protein contaminants in these fractionated samples was 3 ± 1%. The molar masses were calculated in relation to sodium poly(styrene sulfonate) standards.

SPM measurements

The SPM images were recorded with a Nanoscope IIIa SPM (Digital Instruments, Santa Barbara, Calif.), equipped with an extender electronics module, which enables phase imaging in the tapping mode. Both contact and tapping modes of imaging were used. In the tapping mode, silicon cantilevers with a resonance frequency between 250 and 300 kHz were used. Before engaging the drive frequency was set at about 250 Hz below resonance. After engaging the retrace and trace signals were set to be identical before starting the actual imaging. Unless otherwise mentioned the scan rate was 0.7–1.8 Hz, the free amplitude of tapping 50–60 nm and damping ratio 0.5–0.8. In contact mode, both conventional and sharpened silicon nitride 200-μm cantilevers with a spring constant of 0.12 N/m were used. All images (512 × 512 pixels) were measured in air. The scan size varied between 500 nm and 30 μm. No filtering was used during scanning. The measuring unit was placed on a massive stone table to eliminate external vibrations.

The average phase shift ($\Delta\bar{\phi}$, Eq. 1), the average phase shift roughness (R_g, Eq. 2, standard deviation of $\Delta\bar{\phi}$ values) and the average morphological roughness (R_a, Eq. 3) were calculated for the 128 × 128 pixel (Eqs. 1, 2) or 512 × 512 pixel (Eq. 3) ASCII images using the following equations:

$$\Delta\bar{\phi}\ (\text{deg})\ \text{or}\ \bar{z}\ (\text{nm}) = \frac{1}{MN}\sum_{k=0}^{M}\sum_{l=0}^{N} z(x_k,\ y_l), \tag{1}$$

$$R_g(\text{deg}) = \frac{1}{MN}\sqrt{\sum_{k=0}^{M}\sum_{l=0}^{N}\left[z(x_k,\ y_l) - \Delta\bar{\phi}\right]^2}, \tag{2}$$

$$R_a(\text{nm}) = \frac{1}{L_x L_y}\int_0^{L_x}\int_0^{L_y} |f(x,\ y)|\ \mathrm{d}x\ \mathrm{d}y, \tag{3}$$

where M and N are the number of pixels in the x or y direction, $z(x_k, y_l)$ is the current phase-shift (degrees) value at the surface point (x, y), $f(x, y)$ is the surface relative to the centre plane and L_x, and L_y are the dimensions of the surface.

Results and discussion

Morphology of the lignin samples

The imaging was started by studying the morphology of KPRL as a reference sample. A typical surface topograph of KPRL fractionated according to molar mass is shown in Fig. 1a. The surface structure was mostly granular and homogeneous as regards friction. The mean volume of the grains was of the order of 10^5 nm^3 [distribution about $\pm 10^2$ nm^3, including the error (overestimation) arising from the tip–sample convolu-

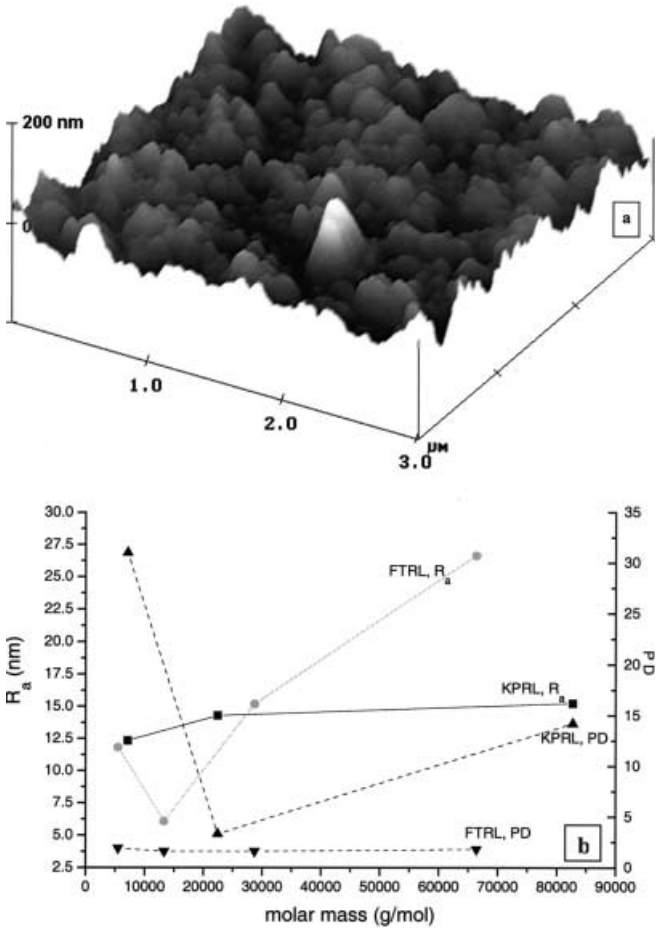

Fig. 1 **a** A scanning probe microscope (*SPM*) topographic image of residual lignin (*RL*) isolated from kraft pulp (*KP*) (*KPRL*) and **b** the topographical roughness and polydispersity (*PD*) values of flow-through RL (*FTRL*) and KPRL as a function of molar mass

tion effect]. Compared with the theoretical 3D model of lignin proposed by Jurasek [33], suggesting that a lignin molecule of $M_w = 54600$ (DP = 300) would have a diameter of some 20 nm, a structure with a volume of 10^5 nm^3 (diameter about 80 nm) would contain about 100 lignin molecules. These observations are consistent with previous scanning electron microscope images of both wood and pulp lignin on a micrometre, scale which also revealed particles quite comparable in size and shape [34, 35]. Because it has been found that RLs of KPs are linked to different carbohydrates in the pulp [30, 36–39], the RLs obtained by the enzymatic hydrolysis may be regarded as residual lignin–carbohydrate complexes [30]. This may explain the relatively large size of the granular structures. Lignin has also been considered as a statistical polymer in which molecules may form aggregates through physical linkages [1, 8]; however, it should be kept in mind that extraction of lignin from the raw material requires that some linkages be cleaved. This should result in lignin fragments with a molecular weight lower than that of lignin initially bound to the cell wall of wood fibres.

In contrast to KPRL, the surface roughness of FTRL correlated well with the molar mass values. The roughness (R_a) and polydispersity (PD) values are plotted as a function of the molar mass of the respective samples in Fig. 1b. The roughness of the FTRLs increased with increasing molar mass. Only the lowest molar mass fraction deviated from this trend, which is difficult to explain. The smallest molar mass fraction of FTRL had the largest PD value of this series, 1.9, but the PD value deviated relatively little from 1 (PD = 1 if the sample is monodisperse and PD $\gg$1, if the structural units have a large size distribution). The PD values show that KPRL ($3.1 \leq PD \leq 14.2$) was clearly more polydisperse than FTRL and may explain why the roughness of KPRL did not correlate to changes in the molar mass as was the case for FTRL samples. Furthermore, the FTRL fractions should not contain any reprecipitated lignin owing to the cooking procedure.

Although the lignin samples were in general homogeneous as regards friction and phase-contrast images, some linear (nongranular) or lower-friction areas were also observed. Friction and phase-contrast images of the surface of KPRL are shown in Fig. 2. Both images resolved grain boundaries better than the respective height-mode images. A peculiar contrast is seen in the heterogeneous friction image of Fig. 2b featuring areas of high (light) and low (dark) friction. The areas of low friction dominate the surface. The local differences in friction are not due to differences in topography (height) as seen by comparing Fig. 2a and b. The friction contrast thus refers to a material contrast, possibly to carbohydrates or proteins existing in a minority on the sample surface. It cannot be ruled out, however, that the friction contrast would relate to structurally different lignins with mechanically (friction) different properties. On the other hand, in this particular case, the rather homogeneous phase-contrast image (Fig. 2d) refers to a viscoelastically homogeneous material. However, more would be concluded about the viscoelastic inhomogeneity over the surface by thoroughly screening the imaging parameters (free amplitude of tapping, set-point amplitude, frequency, etc.). Shevshenko et al [8] have reported SPM measurements of lignin that did not confirm regular spherical particles as typical of lignin or products of chemical transformations. They reported both spherical particles and wavy and filamentous structures. The conclusion was that the sample preparation and substrate surface might contribute to the micrometre morphology of lignin. In our work images characterized as wavy and filamentous were also observed. Because the diameter of the lignin particles studied here was about 0.1–0.5 mm the influence of the substrate surface on the characteristics of the image was negligible.

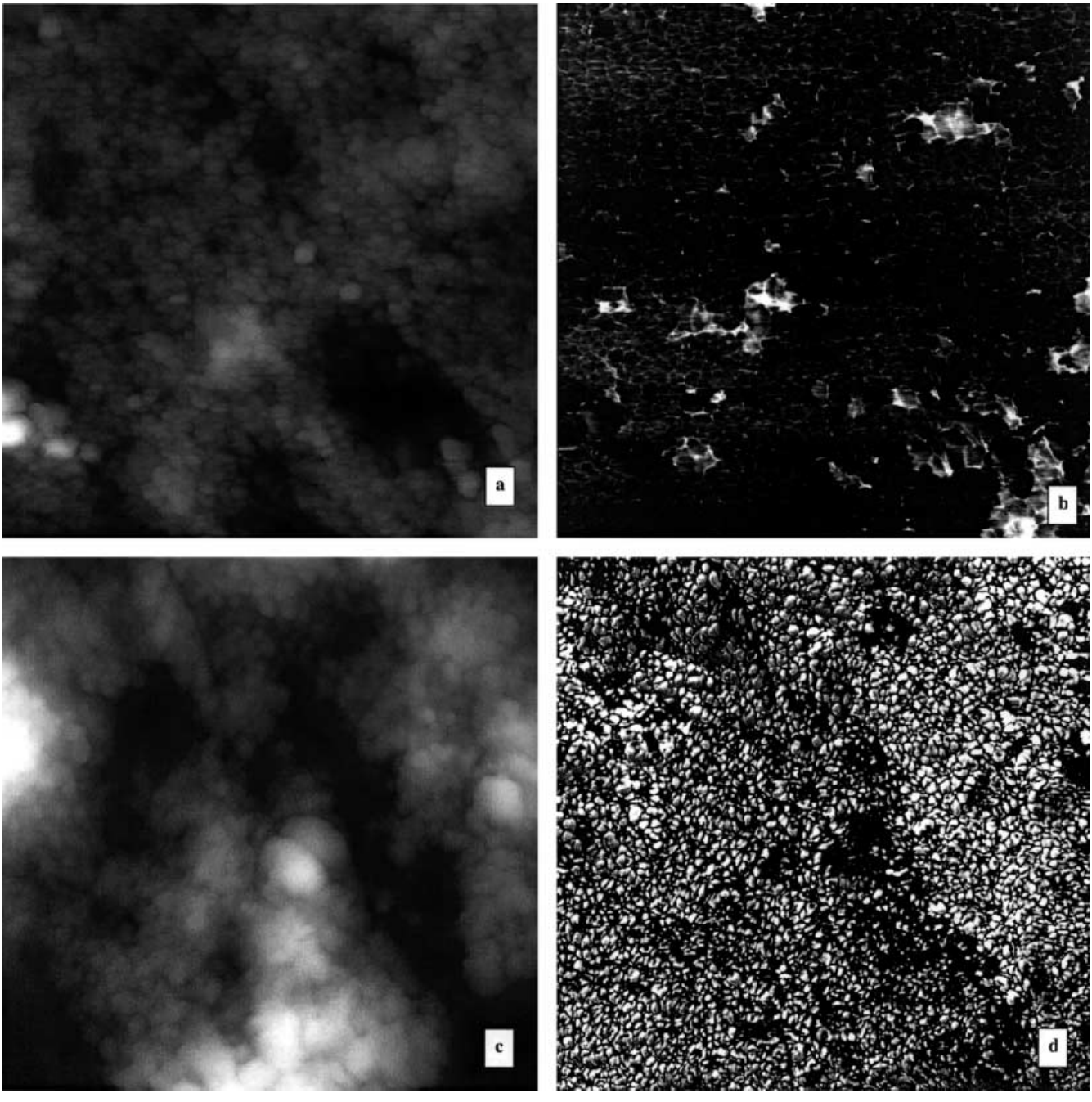

Fig. 2 **a, c** SPM topographic, **b** friction and **d** phase images of KPRL (**a**, **b**: image size 5 μm × 5 μm; **c**, **d**: 2 μm × 2 μm). The z scales for images **a**–**d** are 180 nm, 1.5 V, 180 nm and 120°

Phase-contrast imaging of KP, KPO and BKP

Height and phase images of the KP, KPO and BKP fibre surfaces are shown in Fig. 3. The phase-contrast imaging in the tapping mode was found to be an effective tool to resolve details on the sample surface. This can be observed in all the image pairs of Fig. 3. The phase image clearly resolves the granular (Fig. 3b, d) and the fibrillar (Fig. 3f) fine structure which is not visible in detail in the corresponding topographical images of the same spot.

Both the untreated KP and oxygen-delignified KPO samples had a mostly granular surface structure (about 60–70% and about 80% of the total area of all measured images, respectively). Figure 3b and d shows that the surface of KP and KPO is built up of grains of nonuniform size and form, in contrast to the topographs of Fig. 3a and c, which only resolves the main bundles of microfibrils (diameter about 1 μm and about

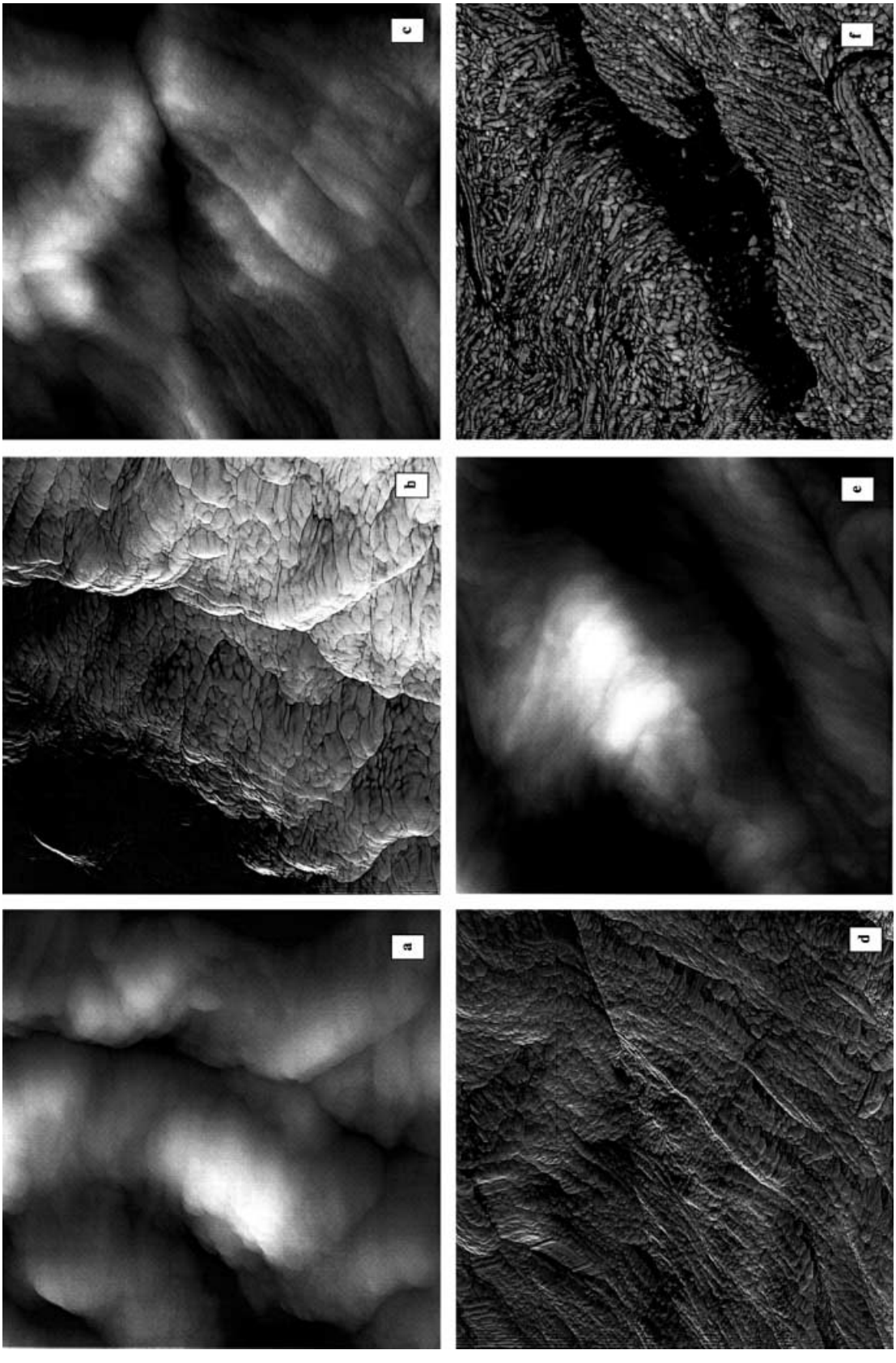
c
f
b
e
a
d

◀

Fig. 3 **a**, **c**, **e** SPM topographic and **b**, **d**, **f** phase images of conventional untreated KP (**a**, **b**: image size 3 μm × 3 μm), oxygen-delignified (**c**, **d**: image size 3 μm × 3 μm) and elemental-chlorine-free-delignified (**e**, **f**: image size 2 μm × 2 μm) pine KP. *z* scales for images **a**–**f** are 685 nm, 33°, 365 nm, 13°, 420 nm and 120°

90–400 nm, respectively). The size of the grains varied for KP samples between 40 and 260 nm and for KPO between 20 and 160 nm (in Fig. 3b between 45 and 250 nm and in Fig. 3d between 20 and 150 nm, respectively). The decreasing size of the grains during oxygen bleaching correlates to earlier observations of higher reactivity of large particles than small ones, since the larger ones have a larger probability to be broken by bleaching chemicals [29]. In addition, the size of the grains of the KP samples correlated well with the dimensions of kraft lignin grains (cf. Fig. 1). This is consistent with the assumption that the RL of KPs contains higher-molar-mass fractions than dissolved kraft lignin and these higher-molar-mass fractions appear at the surface of the fibre wall, which is known to be richer in lignin and pectic substances [40, 41].

ECF delignification removed the granular surface much more effectively than oxygen delignification (about 60–80% of the total area of the measured images was fibrillar). Parallel fibrils of about 45 nm diameter and some small grains of about 40 nm diameter are shown in Fig. 3f. However, in some BKP and KPO samples large (about 250 × 500 nm^2 or even larger, with inhomogeneous form) nonfibrillar structures covered the surface, referring possibly to components reprecipitated from the cooking liquor. The granular structure in our earlier study is suggested to correspond to surface lignin or a mixture of lignin, hemicellulose and extractives since the decrease in the relative amount of the granular phase correlated with a decreasing kappa value of the birch and pine samples of different cooking time [42]. The kappa numbers for the samples studied were now KP, 25.9 (3.885% lignin), KPO, 15.4 (2.31%), BKP, 0 (about 0%). As observed previously by electron spectroscopy for chemical analysis (ESCA) [10] the amount of surface lignin is about 5 times higher (when the total lignin content is greater than 3%) than the amount of bulk lignin. This explains the high amount of the granular surface phase in the KP and KPO samples (Fig. 3b, d). Furthermore, previous ESCA studies by Laine et al [10] have shown that oxygen delignification decreases the surface coverage of lignin by only about 15%, whereas the total lignin reduction is about 50% (from about 4% to about 2%), which is consistent with observations of this study.

The RL of KPs has a lower free phenolic content than dissolved kraft lignin and it is slightly more condensed than native lignin [30]. Lai et al have shown condensed structures to be resistant towards oxygen degradation [43]. Hence, assuming that the properties of RL correlate to surface lignin on the fibre the low amount of free phenolic units on the surface of RL after kraft cooking explains the poor dissolution of surface lignin by oxygen delignification.

Analysis of the phase-shift data

Some colour contrast is visible in the phase-contrast images of Fig 3, referring to an inhomogeneity with respect to surface viscoelasticity. The images of Fig. 3a, b, c, and d and Fig. 3e and f were measured by using a vibrating tip with 60-nm and 40-nm free amplitude, respectively, and a damping ratio, *r*, (set-point/free amplitude) of 0.6–0.8. It is obvious when comparing the topographs and phase-contrast images that the phase-shift data is not connected to any drastic height differences on the surface (Fig. 3a–d); however, the darker area in the phase image of Fig. 3f corresponds to the largest slope and low-surface regions on the surface (cf. Fig. 3e). The smaller free-tapping amplitude (about 40 nm) may give rise to the tip–contamination layer interaction dominating the contrast instead of the pure tip–sample interaction [42]. The dark areas (close to zero or negative phase shift) in the phase-contrast image may, therefore, correspond to regions of higher water content, leading to high tip–sample adhesion forces.

The average phase shift ($\Delta\bar{\phi}$), the average roughness of the phase image (R_g) and the average morphological roughness (R_a) for the KP, KPO, BKP and KPRL samples are shown in Fig. 4 as a function of kappa number. Two different free-tapping amplitudes were chosen in order to follow both the adhesion properties (measured with 30-nm amplitude) and the stiffness properties of the samples (measured with 60-nm amplitude) [16, 19, 42].

When measuring with low free amplitude (30 nm), correlation was observed between the $\Delta\bar{\phi}$, R_g, R_a and proceeding delignification (i.e. the decreasing bulk lignin content, the kappa number) of the samples: the lower the lignin content the more negative the average phase shift. As discussed earlier, a close to zero or a slightly negative phase shift refers to a sticky (e.g. more hydrophilic, high-adhesion) surface when measuring with low free amplitudes [16, 22, 28]. The KP lignin is considered as hydrophobic. Thus, the most negative $\Delta\bar{\phi}$ for the lowest kappa number (i.e. lowest lignin amount, most hydrophilic cellulosic surface) agrees with the assumptions. It has been discussed [16, 20, 22] that measuring with low free amplitude would yield most information about tip–contamination layer interactions (adhesion, amphiphilicity). These results for the KP, KPO, BKP and KPRL samples indicate that the average phase-shift values measured with low tapping amplitude (e.g. 30 nm) may

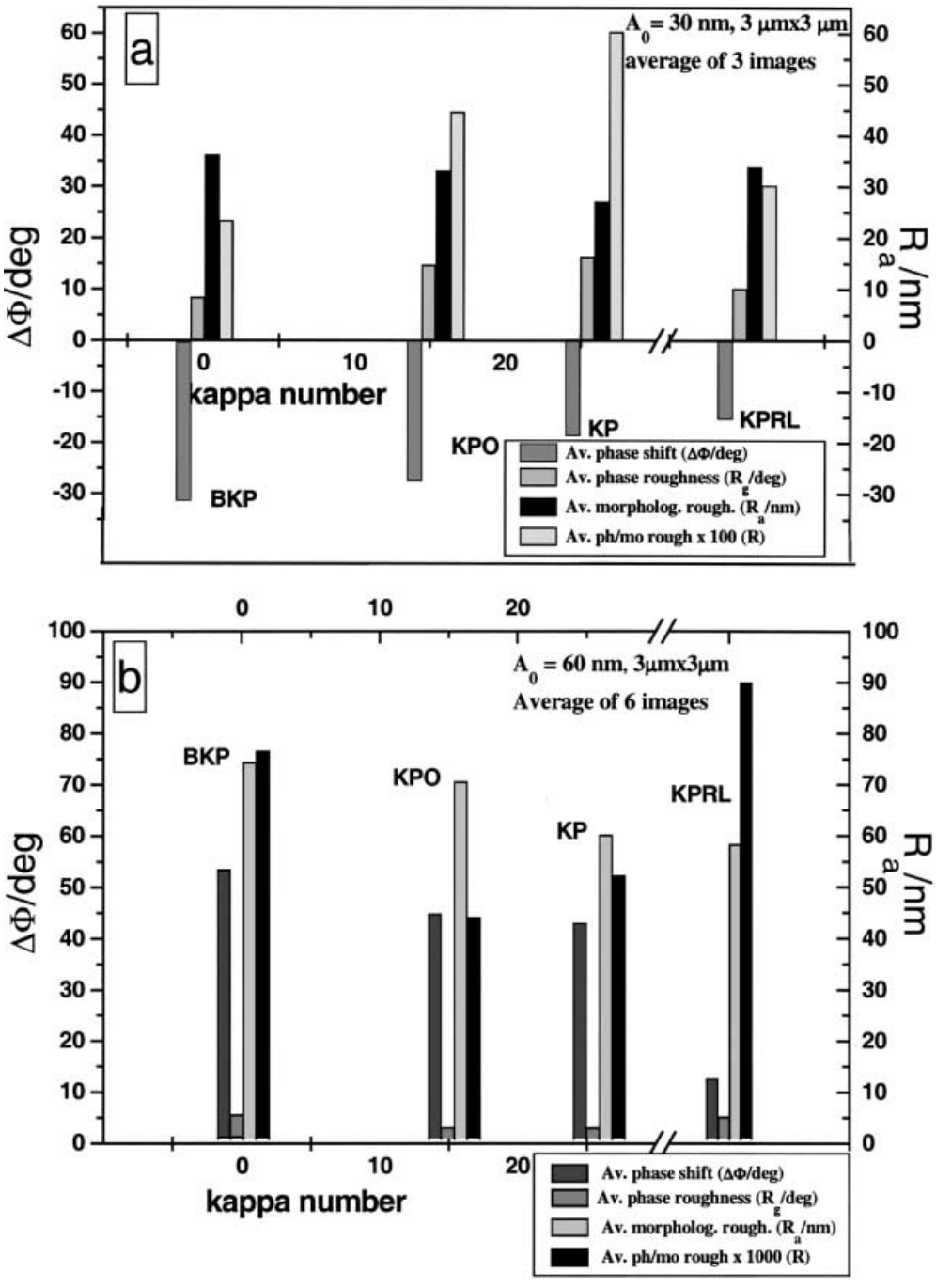

Fig. 4a, b Comparison of KP, oxygen-delignified KP (*KPO*), bleached KP (*BKP*) and KPRL phase-imaging data. Average phase shift, phase and topographical roughness as a function of kappa number for a free tapping amplitude of **a** 30 nm and **b** 60 nm

be used to quantitatively estimate the surface composition of wood fibres with proceeding cooking/delignification.

The R_g value gives the standard deviation of the phase shift values and was taken as a measure of the homogeneity of the surface. The lower the R_g value the more homogeneous the surface properties, i.e. amphiphilicity (for low free amplitudes) or stiffness (for high free amplitudes). The difference in R_g between the KP and KPO samples and also between the BKP and KPRL samples is shown in Fig. 4a. The phase-shift data give the lowest R_g values for the BKP and KPRL samples. BKP and KPRL also appeared most homogeneous regarding the surface texture (fibrillar versus granular) in the phase images. The result is very logical since KPRL should represent pure lignin and BKP, a lignin-free sample.

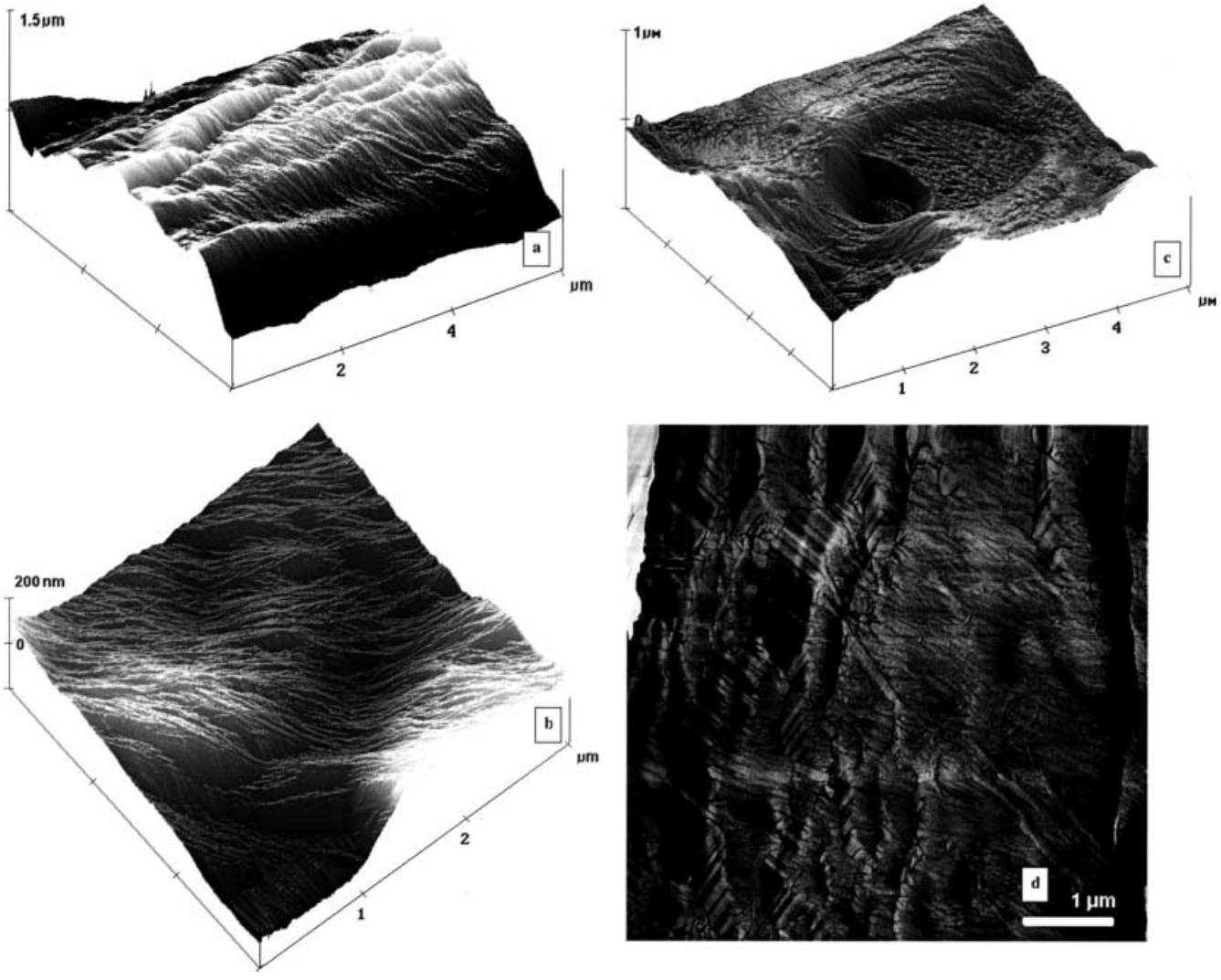

Fig. 5a–d SPM contact-mode-height images of conventional pine KP samples. Surface of **a** a KPO fibre (6 μm × 6 μm) and **b** BKP (3 μm × 3 μm). **c** An example of a cell aperture (5 μm × 5 μm). **d** A friction image of KPO (6 μm × 6 μm, *z* scale 1 V)

To account for the effect of morphological roughness on R_g, the phase-shift roughness normalized to topography, $R = R_g/R_a$, was calculated. Now the trend, the lower the R value the more homogeneous the surface, was seen even more clearly. R decreased linearly from KP to BKP.

In addition, it was found that the surface morphological roughness increased as a function of decreasing kappa value, which is consistent with the breakup of the fibre structure as a function of proceeding delignification. This effect was also seen, even if it was slightly weaker, when measuring the samples with a free tapping amplitude of 60 nm (Fig. 4b).

When measuring with the larger tapping amplitude the contribution arising from the sample stiffness is expected to be the dominating source of contrast in the phase image. The more positive the phase shift the stiffer (harder) the surface, when $r_{sp} > 0.3$ [42]. The results for samples measured with a free amplitude of 60 nm are shown in Fig. 4b. The BKP sample gave the largest $\Delta\bar{\phi}$ value and the KPRL sample the smallest one. Since BKP was found to be mostly fibrillar, consisting most obviously of cellulose, the result of the highest stiffness for BKP compared with the amorphous and softer lignin is logical. The normalized phase-shift roughness, R, however, had an opposite trend compared with the data obtained for the low tapping amplitude.

Comparison of KP, KPO and BKP with contact-mode imaging – topography of wood fibre surfaces

The diameter of the bundles of KP fibrils was about 2–4 μm. A certain linear structure at an angle of 50–60° to the bundle axis (the width of these structures being about 200–400 nm) was often visible. In Fig. 5a of the

KPO sample (6 μm × 6 μm) this linear structure is resolved and appears to consist of fibrils with a width of about 80–100 nm. The diameter of the bundles of fibrils varies between 0.4 and 0.9 μm. Further in Fig. 5b of BKP (3 μm × 3 μm), parallel fibrils of the order of 20–40 nm in diameter can be clearly seen. In conclusion, the proceeding delignification results in a breakup of the bundles of microfibrils into smaller units and eventually details close to individual microfibrils can be resolved.

Higher resolution 1 μm × 1 μm images of the KP sample showed collections of roughly parallel fibrils with a diameter of the order of 0.2–0.3 μm. Accounting for the tip–sample convolution effect [6, 44] the physical diameter for the KP fibrils was estimated to be about 0.1 μm. This size is consistent with a bundle of microfibrils, possibly coated with hemicellulose or lignin.

Cell wall pits were frequently observed (Fig. 5c). Their typical diameter was about 1.5–2.5 μm with a depth of 0.2 μm. The friction image (not shown) did not indicate any difference in material properties between the torus and the bottom of the wall pit aperture. In fact, the FFM images of the pulp samples did not show clear material contrast (Fig. 5d).

Conclusions

The topography of residual lignin, isolated from the conventional and flow-through pine KP was found to be mostly granular. Certain inhomogeneities in the friction images of lignin referred to protein or extractive residues in the sample or, alternatively, to different forms of coexisting lignin. The surface roughness of the flow-through residual lignin samples correlated quite well with the molar mass of the respective fraction. No correlation, on the other hand, was found for the fractionated KP residual lignin.

A granular surface was also observed for the original KP and the oxygen-delignified samples. The ECF delignification was much more effective in removing lignin especially from the surface of pine pulp compared with oxygen delignification.

The SPM allowed straightforward observation of structural features of the fibres, such as pits and individual microfibrils. It was found that the phase-imaging mode was the most informative when compared with the contact-mode height and friction modes of imaging. The data analysis of the average phase shift, the average phase-shift roughness and the average topographical roughness measured using different tapping mode imaging parameters enabled us to study both the surface amphiphilicity and the stiffness of the samples as a function of delignification. This analysis enabled us to distinguish between the changes in the chemical and mechanical properties on the fibre surface with proceeding delignification. However, it was still difficult to unambiguously identify all the various chemical components on the sample surface. Therefore, this study will be expanded in a forthcoming SPM study of model compounds and wood fibres being imaged through systematic variation of the measuring parameters in various environments.

Acknowledgement This work was supported financially by the Academy of Finland.

References

1. Fengel D, Wegener G (1989) Wood chemistry, ultrastructure, reactions. de Gruyter, Berlin
2. Sjöström E (1992) Wood chemistry – fundamentals and applications, vol 2. Academic, San Diego
3. Sugiyama J, Vuong R, Chanzy H (1991) Macromolecules 24:4168–4175
4. Heiner AP, Sugiyama J, Teleman O (1995) Carbohydr Res 273:207–223
5. Baker AA, Helbert W, Sugiyama J, Miles M (1997) J Struct Biol 119: 129–138
6. Kuutti L, Peltonen J, Pere J, Teleman O (1995) J Microsc 178:1–6
7. Hanley SJ, Revol J-F, Godbout L, Gray DG (1997) Cellulose 4:209–220
8. Shevchenko SM, Bailey GW, Shane YY, Akim LG (1996) Tappi J 70: 227–237
9. Sarkanen KV, Ludwig CH (eds) (1971) Lignins – occurrence, formation, structure and reactions. Wiley Interscience, New York
10. Laine J (1996) PhD thesis. Laboratory of Forest Products Chemistry, Espoo
11. (a) Binning G, Quate CF, Gerber C (1986) Phys Rev Lett 56:930–933; (b) Mate CM, McClelland GM, Erlandsson R, Chiang S (1987) Phys Rev Lett 59:1942–1945
12. Meyer G, Amer NM (1990) Appl Phys Lett 57:2089–2091
13. Bhushan B, Isrelachvili JN, Landman U Nature 374:607–616
14. Overney RM, Meyer E, Frommer J, Brodbeck C, Lüthi R, Güntherodt H-J, Fujihira M, Takano H, Gotoh Y (1992) Nature 359:133–135
15. Bar G, Thomann Y, Brandsch R, Cantow HJ, Whangbo MH (1997) Langmuir 13:3807
16. Whangbo MH, Bar G, Brandsch R (1998) Appl Phys A 66:S1267
17. Sarid D, Hunt JP, Workman RK, Yao X, Peterson CA (1998) Appl Phys A 66:S283
18. García R, Tamayo J, Calleja M, García F (1998) Appl Phys A 66:S309
19. Whangbo MH, Magonov SN, Bengel H (1997) Probe Microsc 1:23
20. Tamayo J, García R (1996) Langmuir 12:4430
21. Leclère P, Lazzaroni R, Brédas JL, Yu JM, Dubois P, Jérme R (1996) Langmuir 12:4317
22. Brandsch R, Bar G, Whangbo MH (1997) Langmuir 13:6349
23. Spatz JP, Sheiko S, Möller M, Winkler RG, Reineker P, Marti O (1997) Langmuir 13:4699
24. Holmberg M, Berg J, Rasmusson J, Stemme S, Ödberg L, Claesson P (1997) J Colloid Interface Sci 186:369–381

25. Hanley SJ, Gray DG (1994) Holzforschung 48:29–34
26. Hanley SJ, Griasson J, Revol J-F, Gray DG (1992) Polymer 33:4639–4642
27. Pereira DED, Claudio-da-Silva E Jr (1995) Proceedings of the 8th International Symposium on Wood and Pulping Chemistry, Helsinki 1, June 6–9, 1995. Gummerus Kirjapaino Oy, Jyväskylä, pp 467–474
28. Chernoff DA (1995) Proc Microsc Microanal 888–889
29. Lorenzoni DEDP (1998) PhD thesis. Basle
30. Hortling B, Tamminen T, Turunen E (1997) Proceedings of the 9th International Symposium on Wood and Pulping Chemistry, Montreal, Quebec. Technical Section CPPA, p B6-1
31. Hortling B, Tamminen T, Vuorinen T, Tenkanen M, Teleman A, Pekkala O (1995) Proceedings of the 8th International Symposium on Wood and Pulping Chemistry, June 6–9, 1995, Helsinki 1, vol I. Gummerus Kirjapaino Oy, Jyväskylä, p 231
32. Tamminen T, Hortling B (1999) In: Argyropoulos D (ed) Progress in lignocellulosics characterization. Tappi, Atlanta, pp 1–42
33. Jurasek L (1995) J Pulp Pap Sci 21:J274–J279
34. Mlynar J, Kosikova B, Zakutna L, et al (1990) Cellul Chem Technol 24:475
35. Fengel D (1976) Holzforschung 30:1
36. Minor JL (1991) J Wood Chem Technol 11:150–169
37. Minor JL (1986) J Wood Chem Technol 6:195–201
38. Iversen T, Wännström S (1986) Holzforschung 40:19–22
39. Iversen T, Weatermark U, Samuelsson (1987) Holzforschung 41:119–121
40. Heijnesson A, Simonson R, Westermarck U (1995) Holzforschung 49:313–318
41. Laine J, Stenius P, Carlsson G, Ström G (1994) Cellulose 1:145
42. Simola J, Malkavaara P, Alén R, Peltonen J (2000) Polymer 41:2121–2126
43. Lai Y-Z, Funaoka M, Chen H-T (1994) Holzforschung 48:355
44. Butt H-J, Guckenberger R, Rabe JP (1992) Ultramicroscopy 46:375–393